Further analyses of the structural organization of Homo luzonensis teeth: Evolutionary implications

Clément Zanolli, Yousuke Kaifu, Lei Pan, Song Xing, Armand Mijares, Ottmar Kullmer, Friedemann Schrenk, Julien Corny, Eusebio Dizon, Emil Robles, et al.

Further analyses of the structural organization of *Homo luzonensis* teeth: Evolutionary implications

Clément Zanolli[a,*], Yousuke Kaifu[b], Lei Pan[c,d,1], Song Xing[c,d], Armand S. Mijares[e,f], Ottmar Kullmer[g,h], Friedemann Schrenk[g,h], Julien Corny[i], Eusebio Dizon[f], Emil Robles[e], Florent Détroit[i,*]

[a] *Univ. Bordeaux, CNRS, MCC, PACEA, UMR 5199, F-33600 Pessac, France*
[b] *The University Museum, The University of Tokyo, Tokyo, 113-0033, Japan*
[c] *Key Laboratory of Vertebrate Evolution and Human Origins, Institute of Vertebrate Paleontology and Paleoanthropology, Chinese Academy of Sciences, Beijing, 100044, China*
[d] *CAS Center for Excellence in Life and Paleoenvironment, Beijing, 100044, China*
[e] *Archaeological Studies Program, University of the Philippines, Quezon City 1101, Philippines*
[f] *National Museum of the Philippines, Manila 1000, The Philippines*
[g] *Division of Palaeoanthropology, Senckenberg Research Institute and Natural History Museum Frankfurt, Frankfurt, Germany*
[h] *Department of Palaeobiology and Environment, Institute of Ecology, Evolution, and Diversity, Goethe University Frankfurt, Frankfurt, Germany*
[i] *UMR 7194, CNRS, Département Homme & Environnement, Muséum National d'Histoire Naturelle, Musée de l'Homme, 75016 Paris, France*

*Corresponding authors.
E-mail addresses: clement.zanolli@gmail.com (C. Zanolli); florent.detroit@mnhn.fr (F. Détroit).

[1] Deceased May 2020.

Abstract

The species *Homo luzonensis* has recently been described based on a set of dental and post-cranial elements found at Callao Cave (Northern Luzon, Philippines) and dated to at least 50–67 ka. Seven post-canine maxillary teeth are attributed to this taxon, five of them belonging to the same individual (CCH6) and representing the holotype of *H. luzonensis*, while the isolated upper

premolar CCH8 and the upper third molar CCH9 are paratypes of the species. The teeth are characterized by their small dimensions associated with primitive features, as also found in *Homo floresiensis*, another hominin having evolved in an insular environment of Southeast Asia. Postcranial bones of the hands and feet of *H. luzonensis* and *H. floresiensis* show *Homo habilis*-like or australopith-like features, while cranial and dental morphology are more consistent with the Asian *Homo erectus* morphology. Due to this mosaic morphology, the origin and phylogenetic relationships of both *H. luzonensis* and *H. floresiensis* are still debated. To test the hypotheses that *H. luzonensis* derives from *H. erectus* or from an earlier small-brained hominin, we analyzed the microCT scans of the teeth. We investigated both external and internal tooth structure using morphometric methods including: crown outline shape, tooth crown tissue proportions, enamel-dentine junction shape and pulp morphology. *Homo luzonensis* external crown morphology aligns more with *H. erectus* than with *H. habilis/Homo rudolfensis*. The internal structural organization of *H. luzonensis* exhibits more affinities with that of *H. erectus* and *H. floresiensis* than with Neanderthals and modern humans. Our results suggest that both *H. floresiensis* and *H. luzonensis* likely evolved from some *H. erectus* groups that dispersed in the various islands of this region and became isolated until endemic speciation events occurred at least twice during the Pleistocene in insular environments.

Keywords: Insular evolution; Southeast Asia; endemism; *Homo luzonensis*; *Homo floresiensis*; *Homo erectus*

1. Introduction

1.1. Pleistocene hominin dispersals in the Philippines

Until the beginning of the 2000s, the earliest evidence of human occupation in the Philippines was the modern human frontal bone from Tabon Cave, on the island of Palawan in the southwest of the Philippines, and dated to ca. 16.5 ka (Dizon et al., 2002). Following new excavations and the discovery of more human remains at Tabon Cave, the date of earliest presence of modern humans reaching the East of the Wallace's Line modified by Huxley was pushed back to 47 ± 11 ka (Détroit et al., 2004). However, no older evidence of human presence was known elsewhere in the Philippines. In 2007, the discovery of a third metatarsal (CCH1) at Callao Cave in Northern Luzon, in the Philippines, directly dated by uranium-series ablation to a minimum age of 66.7 ± 1 ka, represented the oldest evidence for the presence of *Homo* in the archipelago (Mijares, 2007). Despite the small size and unusual morphology of the Callao foot bone, it was first considered as compatible with a small-bodied modern human individual (Mijares et al., 2010). The discovery in 2014 of evidence of butchery activities on a large mammal (*Rhinoceros philippinensis*) dating back to 709 ka caused researchers to question the identity of the earliest hominin group(s) to reach the Philippines, as well as the way they reached the archipelago (Ingicco et al., 2018). Land bridges may have formed between the Sunda shelf and the Philippine island of Palawan during the glacial periods of the Middle Pleistocene, facilitating exchanges of fauna, including hominins (Robles et al., 2015). However, it was probably not the case during the Late Pleistocene. Even if the sea strait between Borneo and Palawan probably did not exceed a few kilometers width, there was no connection between Palawan and Luzon islands (Voris, 2000; Robles et al., 2015). Whether Pleistocene hominins reached the Philippines by foot or crossing a narrow sea strait, it seems highly probable that at least two different species arrived there: one during the late Early to early Middle Pleistocene and that can be hypothesized to be related to either *Homo erectus* or to *Homo floresiensis*, both of them being documented in southeast Asia by 1.1–0.7 Ma (Kaifu et al., 2005a, b; van den Bergh et

al., 2016; Matsu'ura et al., 2020), and a second dispersal toward the middle of the Late Pleistocene by modern humans (Détroit et al., 2004).

1.2. The discovery of Homo luzonensis *and evolutionary implications*

Excavations at Callao Cave conducted from 2011 to 2015 yielded 12 additional penecontemporaneous human remains that were attributed to the species *Homo luzonensis*. These include the right P^3–M^3 belonging to a single individual (CCH6-a to CCH6-e, the holotype of the species), the right P^4 CCH8 (previously attributed to $P^{3/4}$ but here assigned to a P^4 based on similarities between CCH8 and CCH6-d enamel-dentine junction morphology; Détroit et al., 2019), the right M^3 CCH9, two adult manual phalanges (CCH2 and CCH5), two adult pedal phalanges (CCH3 and CCH4) and a juvenile femoral shaft (CCH7; Détroit et al., 2019). The teeth are characterized by small dimensions (in the lower part of the range of modern human variation), modern-like simplified crown morphology, relatively large premolars compared to the molars, as well as by the primitive-looking morphology of the premolar roots (Détroit et al., 2019). Large premolars relative to the molars and three-rooted maxillary premolars (particularly P^3s) are also found in *H. erectus*, even if the latter condition is not common (Détroit et al., 2019; Pan and Zanolli, 2019; Pan et al., 2019). A small dentition with primitive features is also found in *H. floresiensis*, another hominin having evolved in an insular environment of Southeast Asia (Brown and Maeda, 2009; Kaifu et al., 2011, 2015a, b). The potentially earliest members of this species were found at Mata Menge, Flores Island, which is dated to ~700 ka (Brumm et al., 2016; van den Bergh et al., 2016), while the *H. floresiensis* specimens recovered at Liang Bua cave are penecontemporanous to those of *H. luzonensis*, dating between 100 ka and 60 ka (Sutikna et al., 2016). Postcranial bones of the hands and feet of both *H. floresiensis* and *H. luzonensis* show early *Homo*-like or australopith-like features, at least in some parts, possibly suggesting an early

origin for these taxa (Tocheri et al., 2007; Argue et al., 2009, 2017; Jungers, 2013; Détroit et al., 2019; Tocheri, 2019). Conversely, cranial and dental morphology of *H. floresiensis* are more consistent with the hypothesis that it derived from Asian *H. erectus* groups (Kaifu et al., 2011, 2015a; Baab, 2016). This is also likely the case for *H. luzonensis* that exhibits a similar mosaic of dental features, with a simplified and apparently 'modern-like' crown associated with multi-rooted premolars reminiscent of some *H. erectus* s.s. specimens (Détroit et al., 2019).

1.3. Aims of the study

To further examine if *H. luzonensis* derives from *H. erectus* or from an earlier, small-brained form of hominin, we analyzed here the external and internal structure of *H. luzonensis* post-canine teeth using surface and microCT scans. We quantified tooth crown tissue proportions, explored pulp morphological variation, and assessed the crown outline, enamel-dentine junction (EDJ) and pulp chamber shape with geometric morphometric methods (elliptical Fourier analyses for the external outline, diffeomorphic surface matching for the EDJ, and landmarks for the pulp chamber) in *H. luzonensis* and compared these data with those available for *Homo habilis* s.l., *H. erectus* s.l., *H. floresiensis*, Neanderthals, and modern humans.

2. Materials and methods

2.1. Scanning and virtual imaging processing

The specimens CCH6b–CCH6e and CCH8 were scanned at the AST-RX platform of the Muséum national d'Histoire naturelle of Paris, in France, with a GE Sensing & Inspection Technologies phoenix|X-ray v|tome|x L240-180 microCT scanner according to the following parameters: 80–90 kV voltage, 120–350 µA current, angular step of 0.19° over a scan angle of 360°. The final volumes were reconstructed with isotropic voxel sizes of 13.61 to 14.33 µm.

The M^3s (CCH6-a and CCH9) were intentionally preserved from potential X-ray damage that may affect future attempts of dating and ancient DNA analyses (Détroit et al., 2019). Surface scanning using photogrammetry was conducted on CCH9 to get the three-dimensional (3D) surface model of the external morphology (Fig. 1). The series of pictures was taken at the 'imagerie 2D/3D' platform of Musée de l'Homme, in France, and the 3D model was generated using Agisoft PhotoScan Professional v. 1.2.6.2834 (Agisoft LLC, St. Petersburg) and Geomagic Studio v. 2013 (3D Systems, Rock Hill).

Using the commercial software Avizo v. 7.0 (FEI Visualization Sciences Group, Hillsboro) and the freeware ImageJ v. 1.52a (Schneider et al., 2012), a semi-automatic, threshold-based segmentation was carried out following the half-maximum height method (Spoor et al., 1993) and the region of interest thresholding protocol (Fajardo et al., 2002; Coleman and Colbert, 2007). The adhering sediment was virtually removed. The 3D models were generated with a constrained smoothing (Fig. 1).

2.2. Crown outline shape analyses

Occlusal crown contours of maxillary premolars and molars were analyzed by normalized (i.e., size-standardized) elliptic Fourier analysis (EFA). Comparative specimens used for these analyses were *H. habilis* s.l., Early Pleistocene *Homo ergaster* from East Africa, Javanese Early Pleistocene *H. erectus* from Sangiran, and Late Pleistocene *H. floresiensis* (see Supplementary Online Material [SOM] Table S1). Additional analyses were made with the inclusion of a modern human sample, which consists of small-bodied populations from Southeast Asia and Africa (Philippine Negrito, African Pygmy), and other populations from Southeast Asia (prehistoric Vietnam, Malaysia, and Indonesia) and Oceania (New Guinea, Australian/Tasmanian Aborigine; for more details, see Kaifu et al., 2015a: S2 Table).

Occlusal crown contours of the *H. luzonensis* specimens were extracted from their 3D surface models created from the CT scans as viewed from infinite distance, using the Meshlab v. 2020.06 software (Cignoni et al., 2008). Those for the comparative specimens were taken from standardized photographs of high-quality plaster casts. A 100 macro lens was used for the photography to minimize parallax effect as detailed in Kaifu et al. (2015a). In cases where interproximal wear on a tooth was minimal and the original occlusal contour could be assessed confidently with reference to the surrounding unworn enamel, we manually reconstructed the contour. If a specimen showed interproximal wear to a degree that was too severe to ensure confident manual reconstruction, we omitted it from the analysis (for example, we excluded the CCH6-d P^4 because mesial wear was slightly too severe with respect to our criteria; Fig. 2A). The contours of the comparative specimens were taken from the better-preserved side. Comparisons were made on the images from the right teeth or horizontally flipped images of the left teeth. The crown contour of each tooth was captured with a tooth placed so that its cervical line is horizontal (whenever a marked enamel extension was present, it was not taken into account to orientate the cervical reference plane). To compute normalized elliptical Fourier descriptors (EFDs), each premolar crown was aligned along the long axis of its first ellipse, and each molar crown was aligned along its mesiodistal axis. Elliptical Fourier descriptors and principal component analyses (PCA) of the normalized EFDs were conducted using the software SHAPE v. 1.3 (Iwata and Ukai, 2002).

2.3. Enamel thickness indices

Among the *H. luzonensis* teeth, only the M^2 CCH6-b exhibits a moderate occlusal wear degree, without any apparent dentine patch (Fig. 1) and is suitable for the assessment of 2D and 3D enamel thickness indices.

Both 2D average and relative enamel thickness (AET and RET) were computed following a protocol originally devised for histological sections (Martin, 1985). To avoid overestimating tooth crown tissues area due to obliquity, a best-fit plane was defined at the cervix of the 3D models in Avizo and the perpendicular virtual buccolingual section passing through the tips of the mesial dentine horns was saved (Benazzi et al., 2014). Following Smith et al. (2008), the reconstruction of the worn outer enamel surface was made prior to measurement based on the curvature and orientation of the outer enamel surface relative to the EDJ (SOM Fig. 1). The following variables then were measured on the section: enamel area (c) and dentine area including the pulp (b), both in mm^2, as well as the EDJ length (d), in mm. We calculated the average enamel thickness (AET = c/d) and the relative enamel thickness (RET = 100 × AET / $[b^{1/2}]$; Martin, 1985).

The 3D average and relative enamel thickness (3D AET and 3D RET) were assessed following Olejniczak et al. (2008). We used Avizo to find the plane halfway between that containing the most apical continuous ring of enamel and that containing the most apical enamel, and defined it as the cervical plane. The crown was virtually separated from the roots at the level of the cervical plane and the following variables were measured or calculated: volume of the enamel cap (Ve), in mm^3; volume of the coronal dentine, including the coronal aspect of the pulp chamber (Vcdp), in mm^3; EDJ surface area (SEDJ), in mm^2; 3D average enamel thickness (3D AET = Ve/SEDJ), in mm; scale-free 3D relative enamel thickness (3D RET = 100 × 3D AET / $[Vcdp^{1/3}]$; see Kono, 2004; Olejniczak et al., 2008).

Each set of measurements was repeated in three alternative days, intra-observer error resulted in <4% differences.

2.4. Enamel-dentine junction shape analyses

We used a diffeomorphic surface matching (DSM) approach to analyze the EDJ conformation. Diffeomorphic surface matching analyses can capture the taxonomically relevant aspects of the EDJ morphology, including both prominent features (such as the dentine horns and marginal crests) and more subtle features (like the protostylid and occlusal basin morphology), and thus improves on traditional (semi)landmark-based geometric morphometric analyses (Beaudet et al., 2016; Zanolli et al., 2018; Braga et al., 2019). This landmark-free, mesh-based approach relies on the construction of average surface models, and the difference between surfaces is interpreted as the amount of deformation needed to align them by using diffeomorphic shape matching (Glaunès and Joshi, 2006; Durrleman et al., 2014). The deformations between surfaces are mathematically modeled as smooth and invertible functions (i.e., diffeomorphisms). From a set of surfaces, an atlas of surfaces is created. The method estimates an average object configuration or mean shape from a collection of object sets (here the EDJ surfaces) and computes the deformations from the mean shape to each specimen. In addition, a set of initial control points located near its most variable parts, and a set of momenta parameterizing the deformations of the mean shape to each individual are estimated (Durrleman et al., 2012).

For each dental position, the EDJ surfaces decimated to 50,000 polygons were manually oriented, then superimposed using the rigid and uniform scale option of the 'Align Surfaces' module in Avizo. This was done by minimizing the root mean square distance between the points of each specimen to corresponding points on the reference surface using an iterative closest point algorithm. We used the Deformetrica v. 4.3 software (Bône et al., 2018) to generate a global mean shape with a set of diffeomorphisms relating the global mean shape to each individual and the output (control points and deformation momenta) used to perform the statistical analyses to explore the EDJ shape variation and to classify the data. The output data were imported in R with

the package 'RToolsForDeformetrica' v. 0.1 (Dumoncel, 2021). Using the packages 'ade4' v. 1.7-6 (Dray and Dufour, 2007) and 'Morpho' v. 2.8 (Schlager, 2020) for R v. 4.0.4 (R Core Team, 2021), we first computed PCAs, followed by between-group PCAs (bgPCA) based on the deformation moments and using the following three groups assigned with equal prior probabilities: *H. erectus* s.l., Neanderthals, and modern humans (SOM Table S2). The Callao Cave specimens were then projected a posteriori into the bgPCA morphospace. We followed the recommendations of Cardini and Polly (2020) by computing the cross-validated bgPCA (cv-bgPCA) to assess the validity of the standard bgPCA group discrimination using the package 'Morpho'. We also performed Jackknife cross-validated canonical variates analyses (CVA) using the same groups than for the bgPCA using the R package 'Morpho'. Since CVA computation requires the number of variables to be much smaller than the number of specimens, we computed the CVA based on a subset of the first principal component (PC) scores (between six and 12) showing the highest degree of correct classification (screening the correct classification results and selecting the minimum number of PC scores enabling to reach the optimum of correct classification; Hastie et al., 2009). This choice of the subset of PC scores is a compromise between including a sufficient proportion of overall shape variation and limiting the number of variables to avoid unrealistic and unstable levels of discrimination (Skinner et al., 2009). We also assessed the structure of the data and results of the multivariate analyses to test that group separation is not spurious (Cardini and Polly, 2020). The amount of variance (r^2) explained by group differences in the raw shape data, in both bgPCA and cv-bgPCA scores, and in the CVA scores was estimated by computing a permutational multivariate analysis of variance (MANOVA; 1,000 permutations) based on the Euclidean distance between the means and implementing a Holm correction using the R packages 'vegan' v. 2.5-7 (Oksanen et al., 2020) and 'pairwiseAdonis' v. 0.3 (Martinez Arbizu, 2020).

2.5. Premolar root morphology and pulp canal configuration

Categories to classify external root number and form were established by Abbott (1984) and Wood and Engleman (1988). This classification system was later extended by Moore et al. (2013, 2015, 2016) to combine both the external root traits and internal canal parameters. We use the latter system, with slight modifications made in order to highlight number of roots (see Pan and Zanolli, 2019). The different categories are abbreviated with a number that refers to the number of roots, followed by letter(s) indicating root form/configuration and by a number in subscript that indicate pulp canal configuration: $1R_1$ = no bifurcation, with one root and one canal; $1R(Bf)_{1Bf}$ = a bifid root apex with a single canal that is bifid at the apex; $1R_{2(1B+1L)}$ = single root (fused buccal and lingual branches), with two circular canals, one buccal and one lingual ($_{1B+1L}$); 2R: 1_1B+1_1 L = two roots, one buccal and one lingual (1B+1L), with two circular canals, one buccal and one lingual (double roots but incompletely separated, fully grown root branches are included in this category); 3R: 2_2B+1_1L = three roots, with two buccal and one lingual branch (2B+1L), with three circular pulp canals, two buccal and one lingual.

Multi-rooted premolars were defined on the basis of furcation exceeding 25% of the total root length, from cervix to root apex (even if the roots of the *H. luzonensis* teeth are not complete, it is evident when more than 25% of the root is missing). The evaluation of root and canal types was performed three times by two observers who found the same pattern.

2.6. Pulp chamber shape analyses

For the M^1 CCH6-c (the other post-canine teeth of *H. luzonensis* showing a more simplified pulp chamber with only two or three pulp horns), seven landmarks were set on the pulp chamber roof: four at the apex of the paracone, protocone, metacone, and hypocone pulp horns, and three

at each intermediate lowest point between the paracone and protocone, paracone and metacone, protocone and metacone. We placed landmarks on a comparative sample including *H. erectus* s.l., Neanderthals and modern humans (see SOM Table S2). As illustrated in Figure 6, the pulp chamber of both *H. floresiensis* M^1s is mesiodistally compressed and only shows two pulp horns, precluding the inclusion of this taxon in this analysis. We performed generalized Procrustes analyses, PCA and bgPCA based on Procrustes shape coordinates and using the same groups as for the DSM analyses of the EDJ. The specimen CCH6-c was then projected a posteriori into the bgPCA morphospace. We also computed the cv-bgPCA to assess the validity of the standard bgPCA group discrimination (Cardini and Polly, 2020). Jackknife cross-validated CVAs were conducted using the same groups than for the bgPCA, still using the R package 'Morpho'. The amount of variance (r^2) explained by group differences in the Procrustes data, in both bgPCA and cv-bgPCA scores, and in the CVA scores was estimated with a MANOVA (1,000 permutations) based on the Euclidean distance between the means and implementing a Holm correction.

3. Results

3.1. Crown outline shape

Results of the EFA for each tooth (from P^3 to M^3) are illustrated in Figure 2. In the PCA plots of the P^3 and P^4, *H. habilis* s.l. and *H. erectus* s.l. (African *H. ergaster* and Indonesian *H. erectus*) overlap. The former tends to have a rounder crown outline, while the latter has a more mesiodistally compressed, elliptical shape (Fig. 2B–C). CCH6-e (P^3) and CCH6-d (P^4) are distinct from *H. habilis* s.l. along PC1, occupying the negative end of this axis together with some *H. erectus*/*H. ergaster* specimens.

Crown outline shape analyses of the M^1, M^2, and M^3 separate *H. erectus* s.s. from the African Early Pleistocene *Homo* sample (*H. habilis* s.l. and *H. ergaster*), without or with minimal

overlap. For M^1s and M^3s, along PC1, crowns are more elongated mesiodistally in the African *Homo* sample but more reduced in the Indonesian *H. erectus* sample (Fig. 2D and 2F). Both *H. luzonensis* and *H. floresiensis* show an even more distinctively reduced M^1 crown than other comparative specimens, and *H. luzonensis* shares mesiodistally reduced M^3 crown shape with Indonesian *H. erectus*. For the M^2s, Indonesian *H. erectus* shows a more rectangular crown outline and tends to fall in the positive space of PC1 and PC2, while African Early Pleistocene *Homo* has a more rhomboidal, asymmetric crown outline corresponding to the negative space of both axes. In the PC morphospace illustrated in Fig. 2E, *H. floresiensis* falls within the range of variation exhibited by the former, but *H. luzonensis* is slightly outside the variation of the comparative sample. The overall patterns of between-group variation in premolar and molar crown shapes seen in Figure 2 do not change if the modern human sample is included in the analysis (SOM Fig. S2).

3.2. Enamel thickness indices

The AET and 3D AET values of the *H. luzonensis* M^2 CCH6-b are lower than those of most of Pleistocene and Holocene *Homo*, being in the lowermost range of variation of Neanderthals and modern humans (Table 1). This is consistent with the small dimensions of the Callao specimen since AET and 3D AET are size-related. Conversely, the RET and 3D RET are scale-free indices and enable comparisons of enamel thickness irrespective of tooth size. *Homo luzonensis* exhibits relatively thick enamel, with RET and 3D RET values higher than in the average figures of Neanderthals, but falls well with the large ranges of variation displayed by other fossil *Homo* and modern humans (Table 1).

3.3. Enamel-dentine junction description

The EDJ of the Callao post-canine teeth displays a low topography, with short dentine horns and a sinuous cervical line (Fig. 3). This is similar to the condition of *H. erectus* and *H. floresiensis* teeth, while Neanderthals and modern humans have taller premolar and molar EDJs. The dentine horns of *H. luzonensis* premolars are less peripheral than in Neanderthals, *H. floresiensis* and modern humans, resembling the condition of *H. erectus* s.s. (Fig. 3A, B). In *H. luzonensis* molars, the central basin is small and the dentine horns are buccolingually closely positioned, as found in *H. erectus* s.s., Neanderthals, and *H. floresiensis*, whereas the dentine horns are more peripherally set in modern humans (Fig. 3C, D). In the M^1 and M^2, the crista obliqua is well developed and starts from the lingual marginal ridge distally to the protocone dentine horn tip, runs buccodistally in the first segment, and then goes parallel to the distal ridge to reach the metacone. This pattern is also found in *H. erectus* s.s., Neanderthals, and *H. floresiensis*, but is rarer in modern humans in which the crista obliqua more generally runs from the protocone dentine horn to that of the metacone or is absent.

3.4. Enamel-dentine junction shape

Comparisons between bgPCA and cv-bgPCA plots show a similar degree of discrimination among *H. erectus* s.l., Neanderthals, and modern humans (Fig. 4; SOM Fig. S3). Results of the MANOVA based on the raw data, bgPCA, cv-bgPCA, and CVA scores confirm the high level of discrimination among the three groups for all tooth positions (SOM Table S3). Correct classification for each group and overall classification resulting from the cv-bgPCA and CVA are reported in the SOM Table S4. Collectively, bgPCA, cv-bgPCA ,and CVA analyses are consistent with each other and confirm that the groups observed in the bgPCA and CVA are not spurious.

For both bgPCA and CVA, posterior probabilities of the P^3, P^4, and M^1 of *H. luzonensis* systematically indicate closer shape similarities with *H. erectus* s.l. than with Neanderthals or modern humans (Table 2), sharing with the former a short EDJ associated with a smaller occlusal basin (Figs. 4 and 5). For the M^2 CCH6-b, posterior probabilities of the bgPCA suggest closer affinities with modern humans while in the CVA it is classified with *H. erectus* s.l. (Table 2). This is illustrated in Figures 4D and 5D, showing that the Callao M^2 has a general pattern that is intermediate between those of *H. erectus* s.l. and modern humans, notably due to the reduction of the talon. Interestingly, similar results are also found for *H. floresiensis* (Table 2; Figs. 4 and 5).

3.5. Premolar root structure and postcanine teeth pulp morphology

The *H. luzonensis* P^3 CCH6-e exhibits three branches, two on the buccal side and one on the lingual side, with a pulp canal running along each of them (Figs. 1 and 6; SOM Fig. S4). This corresponds to the 3R: 2_2B+1_1L pattern that is also observed in the *H. erectus* P^3s of the Early Pleistocene specimen Sangiran 7-35 from Indonesia and of the Middle Pleistocene PA832 specimen from Hexian, in China (Table 3). The 3R: 2_2B+1_1L condition has not been recorded thus far in Neanderthals and is only rarely observed in modern humans. In comparison, the two P^3s of the *H. floresiensis* specimen LB1 show a single root with two separate pulp canals (Fig. 6). The two *H. luzonensis* P^4s display a different pattern: CCH6-d has two root branches with a pulp canal in each one (2R: 1_1B+1_1L) and CCH8 show a three-rooted condition (3R: 2_2B+1_1L). While the two-rooted condition is the most commonly recorded in *H. erectus* s.s. and Neanderthals P^4s, and the only one represented in *H. floresiensis* so far, it is less frequent in modern humans (Table 3). The three-rooted pattern is not found in the P^4s of *H. erectus*, Neanderthals, or *H. floresiensis*, and rarely occurs in modern humans. As a side note, three-rooted P^4s are relatively frequent in *Australopithecus* and *Paranthropus* (38% and 82% of P^4s, respectively; Moore et al., 2016).

In terms of overall morphology, the pulp cavity of the *H. luzonensis* teeth resembles more the condition of *H. erectus* s.s. than those of Neanderthals, *H. floresiensis*, and modern humans (Fig. 6). More specifically, the *H. luzonensis* premolars exhibit two pointy pulp horns and a mesiodistally flattened pulp chamber resembling *H. erectus.* Neanderthals have more rounded pulp horns and a proportionally higher chamber. *Homo floresiensis* displays a unique pulp chamber morphology, without marked pulp horns but showing an unusual buccal protrusion. Modern humans have higher pulp horns and chamber, together with a highly mesiodistally flattened chamber. Similarly, *H. luzonensis* M^1 and M^2 pulp morphology closely resembles those of *H. erectus*, *H. floresiensis*, and modern humans with a low chamber associated with sharp pulp horns (except for LB1), as well as flattened and divergent root canals (Fig. 6). Neanderthals are distinguished by a much higher—taurodont—pulp chamber with more rounded horns and more longitudinally oriented canals.

3.6. First molar pulp chamber shape

Comparisons between bgPCA and cv-bgPCA plots show a similar degree of discrimination among *H. erectus* s.l., Neanderthals, and modern human M^1s (Fig. 7; SOM Fig. S5). Results of the MANOVA based on the raw data, bgPCA, cv-bgPCA, and CVA scores confirm the high level of discrimination among the three groups (SOM Table S5). Correct classification for each group and overall classification accuracy resulting from the cv-bgPCA and CVA are high (SOM Table S6). Collectively, bgPCA, cv-bgPCA, and CVA analyses are consistent with each other and confirm that the groups observed in the bgPCA and CVA are not spurious.

As illustrated in Figure 7, in both bgPCA and CVA the M^2 CCH6-c pulp chamber shape is more similar to that of *H. erectus* s.s. than to those of Neanderthals and modern humans. This is

supported by the posterior probabilities calculated for CCH6-c that unambiguously show similarities with *H. erectus* (Table 4).

4. Discussion

The fossil record of *H. luzonensis* currently includes 13 specimens, seven of them representing dental elements and the remaining six being postcranial bones belonging to a juvenile (the femoral shaft CCH7) and to adult individuals (the metatarsal CCH1, and the manual and pedal phalanges CCH2–CCH5; Détroit et al., 2019). In addition to the small dimensions of the specimens, the phalanges and metatarsal bone show a number of archaic-like features such as a longitudinally curved and dorso-palmarly compressed shaft, well-developed flexor sheath attachments, strongly developed dorsal beak, and small base of the articulations compared with the longitudinal length. These bones partly differ from the typical condition of early *Homo*, *Paranthropus*, and Neanderthals, but share similarities with *Australopithecus*, *H. floresiensis*, and, to a lesser extent, modern humans (Mijares et al., 2010; Détroit et al., 2019). Similarly, some postcranial elements of *H. floresiensis* show primitive features reminiscent of *Australopithecus* or early *Homo* (Tocheri et al., 2007), but the interpretation of the nature and polarity (autapomorphy vs. plesiomorphy) of these traits remains debated (Kaifu et al., 2015a, b; Baab, 2016; Argue et al., 2017). In fact, the particular morphology of *H. luzonensis* and *H. floresiensis* hand and foot bones may have resulted from their evolution in insular environments. The extinct and extant vertebrate faunas of the Philippines show high rates of endemism (Heaney et al., 2016; van der Geer et al., 2017), with postcranial morphological aspects resembling the primitive condition shown by earlier members of the lineage (van der Geer, 2005). Indeed, in association with changes of body proportions, evolutionary reversals or novel adaptations have been documented in the limb bone extremities of a number of mammals having evolved on islands, in southeast Asia and elsewhere

(Sondaar, 1991; Caloi and Palombo, 1994; Köhler and Moyà-Solà, 2001; van der Geer, 2005, 2014; van den Hoek Ostende, 2018; Young, 2020). Similar phenomena also could have occurred in *H. floresiensis* and *H. luzonensis*. However, the rarity of African early *Homo* and *H. erectus* s.s. manual and pedal phalanges limits comparisons and testing evolutionary hypotheses.

In the absence of molecular data and/or cranial remains, the well-preserved external and internal structures of the Callao Cave teeth contain valuable paleobiological information, representing the most reliable elements to track evolutionary relationships between *H. luzonensis* and other Pleistocene and extant *Homo* taxa. Indeed, tooth crown outline, as well as EDJ morphology and pulp chamber shape have been previously demonstrated to exhibit a reliable taxonomic signal (Skinner et al., 2008, 2009, 2016; Macchiarelli et al., 2013; Kaifu et al., 2015a; Zanolli et al., 2018, 2019a, b; Pan et al., 2020). Our results indicate that compared with the dentition of *H. habilis*—that retains *Australopithecus*-like features and often bears multiple accessory cusps (Davies et al., 2021)—the external crown morphology of the postcanine teeth of *H. luzonensis* and *H. floresiensis* appears more derived and simplified, similar to that of Indonesian late Early to early Middle Pleistocene *H. erectus* (Fig. 2; SOM Fig. S2). Available data on the internal morphology of *H. habilis* teeth are currently limited to the EDJ of the mandibular teeth (Davies et al., 2021). While there are as yet no mandibular teeth known for *H. luzonensis*, comparisons with the lower molar EDJs of *H. floresiensis* show that the latter are quite distinct in size and shape from those of *H. habilis* and are highly similar to those of late Early to Middle Pleistocene *H. erectus* specimens from the Sangiran Bapang/Kabuh Formation in Java (Fig. 8).

Analyses of the internal structure of *H. luzonensis* and *H. florensiensis* tooth crown (enamel thickness, EDJ morphology) and roots (pulp morphology) give a consistent signal. Only for the P^3s of *H. floresiensis* and for the M^2s of *H. luzonensis* and *H. floresiensis* are the results of the

geometric morphometric analyses of the EDJ more ambiguous (Figs. 4 and 5). For the P^3 of the Liang Bua specimen, this can be explained by the fact that the EDJ has a unique morphology, with peripheral dentine horns and a large basin (but differing from the modern human condition; Kaifu et al., 2015a, b), associated with a short crown (as generally found in *H. erectus*; see Pan et al., 2020). For the M^2s, the overall EDJ morphology of CCH6-b (short dentine horns with a small central basin) is typical of *H. erectus*, but the talon is proportionally smaller than the trigon and the occlusal outline is trapezoidal, giving it to some extent a modern-like aspect (Fig. 3). The EDJ of the *H. floresiensis* M^2s has an even more peculiar morphology, with an *H. erectus*-like central basin shape and a disproportionately large lingual aspect compared with the buccal one, unlike any other specimen included in our analyses (Fig. 3).

Three-rooted maxillary premolars with three pulp canals of two of the three premolars of *H. luzonensis* resemble the morphology found in the *H. erectus* P^3s S7-35 and PA832 (Pan and Zanolli, 2019). Some African Plio-Pleistocene hominins (Moore et al., 2016) and early *Homo* specimens like KNM-ER 1590 (Wood and Engleman, 1988) also exhibit three-rooted maxillary premolars, which are also rarely expressed in modern humans. While the condition of *H. habilis* remains unknown, the rare but occurring three-rooted upper premolars in Pleistocene hominins and recent humans potentially questions the robusticity of this feature as taxonomically diagnostic.

Recent genetic analyses revealed that modern humans from southeast Asia exhibit Denisovan genes in their genome, suggesting that the two groups met and interbred in the region during the Middle to Late Pleistocene (Browning et al., 2018; Jacobs et al., 2019; Larena et al., in press). Denisovans are currently known by three isolated teeth from Denisova Cave (the isolated dP_4 Denisova 2, the $M^{2/3}$ Denisova 4, and the M^3 Denisova 8; Douka et al., 2019), and the right mandibular corpus Xiahe from Baishiya Karst Cave (the specimen preserves the roots of the

anterior teeth, of the P_3, and the complete M_1 and M_2; Chen et al., 2019). The Denisovan permanent molars are characterized by large dimensions, in the range of Early to Middle Pleistocene *Homo* groups but larger than in modern humans (with a mesiodistal diameter ranging from 13.1 mm to 15.1 mm, and a buccolingual diameter ranging from 12.5 to 14.7 mm; Reich et al., 2010; Sawyer et al., 2015; Chen et al., 2019). In comparison, both *H. luzonensis* and *H. floresiensis* molars show substantially smaller crown size, in the lower range of the modern human variation (with a mesiodistal diameter ranging from 7.9 mm to 11.4 mm, and a buccolingual diameter ranging from 8.9 mm to 11.9 mm; Brown et al., 2004; Morwood et al., 2005; Détroit et al., 2019). In addition, Denisovan molars are characterized by a complex crown morphology, including the presence of accessory cusps, occlusal wrinkling, and a marked crista obliqua running diagonally from the protocone to the metacone (Reich et al., 2010; Sawyer et al., 2015). *Homo luzonensis* and *H. floresiensis* molar crowns exhibit a simplified morphology and a low, less prominent crista obliqua that starts distally from the protocone and runs nearly parallel to the mesial marginal crest to reach the metacone (Fig. 1). Both dental dimensions and morphology of *H. luzonensis* and *H. floresiensis* thus strikingly differ from those of the known Denisovan teeth, suggesting that they are not directly related. Even though the Denisovans and modern humans met and interbred in southeast Asia during the Late Pleistocene (Larena et al., in press), whether they have interacted with the endemic hominin taxa remains to be elucidated.

As a whole, our results support the hypothesis that both of these endemic taxa derived from *H. erectus* s.s. and developed some autapomorphies, which is in agreement with their distinction at the species level. The peculiarities of *H. luzonensis* and *H. floresiensis* tooth structural organization are likely related to the reduction of body size and associated reduction of dental dimensions compared with other Pleistocene *Homo* species (Brown et al., 2004; Brown and Maeda, 2009; Détroit et al., 2019). A different but parallel phenomenon is known in modern

humans which exhibit a reduction trend of the jaw and tooth dimensions through the Late Pleistocene (especially affecting the distalmost teeth, the M2 and M3), associated with a morphological simplification of the crown and roots (reduction of the number of cusps and accessory features, fusion of root branches; see Bailey and Hublin, 2013; Scott et al., 2018). It is thus likely that, as in modern humans, a decrease in postcanine tooth size from a *H. erectus*-like pattern was accompanied by a simplification of crown morphology (albeit preserving complex root systems) in both *H. luzonensis* and *H. floresiensis*. However, considering the differences in premolar vs. molar proportions (*H. luzonensis* premolars are proportionally larger than the molars compared with other *Homo* species, including *H. floresiensis*; Détroit et al., 2019: Fig. 3), and external and internal tooth structure, it is likely that the latter two species diverged from distinct *H. erectus* groups during the late Early to Middle Pleistocene. The identification of isolated teeth morphodimensionally similar to those of *H. floresiensis* from the Bapang/Kabuh Formation of Sangiran, in Java (Fig. 8; Zanolli, 2013, 2015), and of ~700 ka *H. floresiensis*-like dentognathic remains dated from Mata Menge, in Flores Island (van den Bergh et al., 2016), suggest that selection for small body size emerged early in some southeast Asian *H. erectus* groups. While no human remains have been described so far, evidence of butchery activity around the same time at Kalinga, located a few tens of kilometers away from Callao Cave (Ingicco et al., 2018), raises questions about the taxonomic identity of this human group that arrived in the Philippines during the late Early to early Middle Pleistocene and about its relationship with *H. luzonensis*.

5. Conclusions

Our results for most tooth positions consistently align *H. luzonensis* external crown morphology more with Indonesian *H. erectus* than with *H. habilis/Homo rudolfensis*. The internal structural organization of *H. luzonensis* teeth exhibits more affinities with that of *H. erectus* and *H.*

floresiensis than with Neanderthals and modern humans (except for the M^2s that show a more intermediate signal). Altogether, the analyses of the external and internal tooth structural organization of *H. luzonensis* teeth support the validity of this taxon, distinguished from African early *Homo*, *H. erectus* s.s., *H. floresiensis*, Neanderthals, and modern humans. These results confirm the taxonomic diversity of Pleistocene hominins in insular Southeast Asia and the role of insular environment in the speciation of *Homo*. They suggest that both *H. floresiensis* and *H. luzonensis* likely evolved from some Asian *H. erectus* groups that dispersed in the various islands of this region and became isolated until endemic speciation events occurred, at least twice during the Pleistocene in these insular contexts.

Acknowledgments

We would like to dedicate this study to our dear friend and colleague Lei Pan who passed away in May 2020. She was a diligent, committed, and esteemed scientist, appreciated for her kindness, humanity, and generosity. We thank the Cagayan Provincial Government and the Protected Area Management Board-Peñablanca for authorizing fieldwork at Callao Cave. We are also indebted to the following institutions: National Museum of the Philippines, University of the Philippines, Pusat Penelitian Arkeologi Nasional, IVPP, Naturalis, Hanoi Institute of Archaeology, Center for Southeast Asian Prehistory, Thai Fine Arts Department, National Research Council of Thailand, Senckenberg Research Institute and Natural History Museum Frankfurt, American Museum of Natural History, Field Museum of Natural History, Ethiopian Authority for Research and Conservation of the Cultural Heritage; National Museums of Kenya and Government of Kenya, Ditsong National Museum of Natural History, Evolutionary Studies Institute, University of the Witwatersrand, MNHN. We express our gratitude to the Werner Reimers Foundation in Bad Homburg, which provides the Gustav Heinrich Ralph von

Koenigswald collection as a permanent loan for scientific research to the Senckenberg Research Institute and Natural History Museum Frankfurt. We also acknowledge the microCT scanning institution and online sharing platforms: AST-RX and Imagerie 2D/3D MH-SU platforms (MNHN), Centre de Microtomographie (Univ. Poitiers), Nespos Society (https://www.nespos.org), ESRF Paleontological Database (https://paleo.esrf.eu). We gratefully acknowledge support from the CNRS/IN2P3 Computing Center (Lyon - France) for providing computing and data-processing resources needed for this work. For access to comparative material and sharing of microCT scans, we are indebted to: P. Bayle, A. Bravin, M. Le Luyer, A. Mazurier, R. Macchiarelli, C. Nemoz, P. Tafforeau. We sincerely thank the Editor-in-Chief (Andrea Taylor), the Guest Editor, and the two anonymous reviewers for their constructive comments that helped to improve a previous version of this paper. This research project was funded by: Wenner Gren Foundation for Anthropological Research International Collaborative Research Grant (Grant No. ICRG–106), Leakey Foundation Research Grant; University of the Philippines Enhanced Creative Work and Research Grant (ECWRG 2015-1- 016), SYNTHESYS grant (NLTAF- 1130), 'IUSS Ferrara 1391' grant, Labex BCDiv 'Biological and Cultural Diversities', Erasmus Mundus IMQP and IDQP, MQPI (MEAE), French CNRS. This study received financial support from the French government in the framework of the University of Bordeaux's IdEx 'Investments for the Future' program / GPR 'Human Past'.

References

Abbott, S.A., 1984. A comparative study of tooth root morphology in the great apes, modern man and early hominids. Ph.D. Dissertation, University of London.

Abella, F., Teixidó, L.M., Patel, S., Sosa, F., Duran-Sindreu, F., Roig, M., 2015. Cone-beam computed tomography analysis of the root canal morphology of maxillary first and second premolars in a Spanish population. J. Endodont. 41, 1241–1247.

Argue, D., Morwood, M.J., Sutikna, T., Jatmiko, Saptomo, E.W., 2009. *Homo floresiensis*: A cladistic analysis. J. Hum. Evol. 57, 623–639.

Argue, D., Groves, C.P., Lee, M.S.Y., Jungers, W.L., 2017. The affinities of *Homo floresiensis* based on phylogenetic analyses of cranial, dental, and postcranial characters. J. Hum. Evol. 107, 107–133.

Baab, K.L., 2016. The place of *Homo floresiensis* in human evolution. J. Anthropol. Sci. 94, 5–18.

Bailey, S.E., Hublin, J.-J., 2013. What does it mean to be dentally "modern"? In: Scott, G.R., Irish, J.D. (Eds.), Anthropological Perspectives on Tooth Morphology. Genetics, Evolution, Variation. Cambridge University Press, Cambridge, 222–249.

Beaudet, A., Dumoncel, J., Thackeray, J.F., Bruxelles, L., Duployer, B., Tenailleau, C., Bam, L., Hoffman, J., de Beer, F., Braga, J., 2016. Upper third molar internal structural organization and semicircular canal morphology in Plio-Pleistocene South African cercopithecoids. J. Hum. Evol. 95, 104–120.

Benazzi, S., Panetta, D., Fornai, C., Toussaint, M., Gruppioni, G., Hublin, J.-J., 2014. Technical Note: Guidelines for the digital computation of 2D and 3D enamel thickness in hominoid teeth. Am. J. Phys. Anthropol. 153, 305–313.

Bône, A., Louis, M., Martin, B., Durrleman, S., 2018. Deformetrica 4: An open-source software for statistical shape analysis. In: Reuter, M., Wachinger, C, Lombaert, H., Paniagua, B., Lüthi, M., Egger, B. (Eds.), Shape in Medical Imaging, International Workshop, ShapeMI

2018 Held in Conjunction with MICCAI 2018 Granada, Spain, September 20, 2018 Proceedings. LCNS Springer, Cham, pp. 3–13.

Braga, J., Zimmer, V., Dumoncel, J., Samir, C., de Beer, F., Zanolli, C., Pinto, D., Rohlf, F.J., Grine, F.E., 2019. Efficacy of diffeomorphic surface matching and 3D geometric morphometrics for taxonomic discrimination of Early Pleistocene hominin mandibular molars. J. Hum. Evol. 130, 21–35.

Brown, P., Maeda, T., 2009. Liang Bua *Homo floresiensis* mandibles and mandibular teeth: A contribution to the comparative morphology of a new hominin species. J. Hum. Evol. 57, 571–596.

Brown, P., Sutikna, T., Morwood, M.J., Soejono, R.P., Jatmiko, Saptomo, E.W., Awe Due, R., 2004. A new small-bodied hominin from the Late Pleistocene of Flores, Indonesia. Nature 431, 1055–1061.

Browning, S.R., Browning, B.L., Zhou, Y., Tucci, S., Akey, J.M., 2018. Analysis of human sequence data reveals two pulses of archaic Denisovan admixture. Cell 173, 53–61.

Brumm, A., van den Bergh, G.D., Storey, M., Kurniawan, I., Alloway, B.V., Setiawan, R., Setiyabudi, E., Grun, R., Moore, M.W., Yurnaldi, D., Puspaningrum, M.R., Wibowo, U.P., Insani, H., Sutisna, I., Westgate, J.A., Pearce, N.J., Duval, M., Meijer, H.J., Aziz, F., Sutikna, T., van der Kaars, S., Flude, S., Morwood, M.J., 2016. Age and context of the oldest known hominin fossils from Flores. Nature 534, 249–253.

Caloi, L., Palombo, M.R., 1994. Functional aspects and ecological implications in Pleistocene endemic herbivores of Mediterranean Islands. Hist. Biol. 8, 151–172.

Cardini, A., Polly, P.D., 2020. Cross-validated between group PCA scatterplots: A solution to spurious group separation? Evol. Biol. 47, 85–95.

Chen, F., Welker, F., Shen, C.-C., Bailey, S.E., Bergmann, I., Davis, S., Xia, H., Wang, H., Fischer, R., Freidline, S.E., 2019. A late Middle Pleistocene Denisovan mandible from the Tibetan Plateau. Nature 569, 409–412.

Cignoni, P., Callieri, M., Corsini, M., Dellepiane, M., Ganovelli, F., Ranzuglia, G., 2008. MeshLab: An open-source mesh processing tool. In: Scarano, V., De Chiara, R., Erra, U. (Eds.), Sixth Eurographics Italian Chapter Conference. The Eurographics Association, Salerno, pp. 129–136.

Coleman, M.N., Colbert, M.W., 2007. Technical note: CT thresholding protocols for taking measurements on three-dimensional models. Am. J. Phys. Anthropol. 133, 723–725.

Davies, T.W., Alemseged, Z., Gidna, A., Hublin, J.-J., Kimbel, W.H., Kullmer, O., Spoor, F., Zanolli, C., Skinner, M.M., 2021. Accessory cusp expression at the enamel-dentine junction of hominin mandibular molars. PeerJ 9, e11415.

Détroit, F., Dizon, E., Falguères, C., Hameau, S., Ronquillo, W., Sémah, F., 2004. Upper Pleistocene *Homo sapiens* from Tabon Cave (Palawan, The Philippines): Description and dating of new discoveries. C. R. Palevol. 3, 705–712.

Détroit, F., Mijares, A.S., Corny, J., Daver, G., Zanolli, C., Dizon, E., Robles, E, Grün, R., Piper, P.J., 2019. A new species of *Homo* from the Late Pleistocene of the Philippines. Nature 568, 181–186.

Dizon, E., Détroit, F., Sémah, F., Hameau, S., Ronquillo,W., Cabanis, E., 2002. Notes on the morphology and age of the Tabon Cave fossil *Homo sapiens*. Curr. Anthropol. 43, 660–666.

Douka, K., Slon, V., Jacobs, J., Bronk Ramsey, C., Shunkov, M.V., Derevianko, A.P., Mafessoni, F., Kozlikin, M.B. Li, Bo, Grün, R., Comeskey, D. Devièse, T., Brown, S., Viola, B., Kinsley, L., Buckley, M., Meyer, M., Roberts, R.G., Pääbo, S., Kelso, J., Higham, T., 2019.

Age estimates for hominin fossils and the onset of the Upper Palaeolithic at Denisova Cave. Nature 565, 640–644.

Dray, S., Dufour, A., 2007. The ade4 package: Implementing the duality diagram for ecologists. J. Stat. Softw. 22, 1–20.

Dumoncel, J., 2021. RToolsForDeformetrica. R package version 0.1. https://gitlab.com/jeandumoncel/tools-for-deformetrica/-/tree/master/src/R_script/RToolsForDeformetrica.

Durrleman, S., Pennec, X., Trouvé, A., Ayache, N., Braga, J., 2012. Comparison of the endocranial ontogenies between chimpanzees and bonobos via temporal regression and spatiotemporal registration. J. Hum. Evol. 62, 74–88.

Durrleman, S., Prastawa, M., Charon, N., Korenberg, J.R., Joshi, S., Gerig, G., Troué, A., 2014. Morphometry of anatomical shape complexes with dense deformations and sparse parameters. NeuroImage 101, 35–49.

Fajardo, R.J., Ryan, T.M., Kappelman, J., 2002. Assessing the accuracy of high-resolution X-ray computed tomography of primate trabecular bone by comparisons with histological sections. Am. J. Phys. Anthropol. 118, 1–10.

Glaunès, J., Joshi, S., 2006. Template estimation from unlabeled point set data and surfaces for computational anatomy. In: Pennec, X., Joshi, S. (Eds.), Proceedings of the International Workshop on the Mathematical Foundations of Computational Anatomy. LNCS Springer, Copenhagen, pp. 29–39.

Hastie, T., Tibshirani, R., Friedman, J., 2009. The Elements of Statistical Learning, 2nd ed. Springer, New York.

Heaney, L.R., Balete, D.S., Rickart, E.A., 2016. The Mammals of Luzon Island. Johns Hopkins University Press, Baltimore.

Ingicco, T., van den Bergh, G.D., Jago-on, C., Bahain, J.-J., Chacón, M.G., Amano, N., Forestier, H., King, C., Manalo, K., Nomade, S., Pereira, A., Reyes, M.C., Sémah, A.-M., Shao, Q., Voinchet, P., Falguères, C., Albers, P.C.H., Lising, M., Lyras, G., Yurnaldi, D., Rochette, P., Bautista, A., de Vos, J., 2018. Earliest known hominin activity in the Philippines by 709 thousand years ago. Nature 557, 233–237.

Iwata, H, Ukai, Y., 2002. SHAPE: A computer program package for quantitative evaluation of biological shapes based on elliptic Fourier descriptors. J. Heredity 93, 384–385.

Jacobs, G.S., Hudjashov, G., Saag, L., Kusuma, P., Darusallam, C.C., Lawson, D.J., Mondal, M., Pagani, L., Ricaut, F.-X., Stoneking, M., Metspalu, M., Sudoyo, H., Lansing, J.S., Cox, M.P., 2019. Multiple deeply divergent Denisovan ancestries in Papuans. Cell 177, 1010–1021.

Jungers, W.L., 2013. *Homo Floresiensis*. In: Begun, D.R. (Ed.), A Companion to Paleoanthropology. John Wiley & Sons, Chichester, pp. 582–598.

Kaifu, Y., Aziz, F., Baba, H., 2005a. Hominid mandibular remains from Sangiran: 1952–1986 collection. Am. J. Phys. Anthropol. 128, 497–519.

Kaifu, Y., Baba, H., Aziz, F., Indriati, E., Schrenk, F., Jacob, T., 2005b. Taxonomic affinities and evolutionary history of the Early Pleistocene hominids of Java: Dentognathic evidence. Am. J. Phys. Anthropol. 128, 709–726

Kaifu, Y., Baba, H., Sutikna, T., Morwood, M.J., Kubo, D., Saptomo, E.W., Jatmiko, Awe, R.D., Djubiantono, T., 2011. Craniofacial morphology of *Homo floresiensis*: Description, taxonomic affinities, and evolutionary implication. J. Hum. Evol. 61, 644–682.

Kaifu, Y., Kono, R., Sutikna, T., Saptomo, E.W., Jatmiko, Awe, R.D., 2015a. Unique dental morphology of *Homo floresiensis* and its evolutionary implications. PLoS One 10, e0141614.

Kaifu, Y., Kono, R., Sutikna, T., Saptomo, E.W., Jatmiko, Awe, R.D., Baba, H., 2015b. Descriptions of the dental remains of *Homo floresiensis*. Anthropol. Sci. 123, 129–145.

Köhler, M., Moyà-Solà, S., 2001. Phalangeal adaptations in the fossil insular goat *Myotragus*. J. Vert. Paleontol. 21, 621‑624.

Kono, R., 2004. Molar enamel thickness and distribution patterns in extant great apes and humans: new insights based on a 3-dimensional whole crown perspective. Anthropol. Sci. 112, 121–146.

Larena, M., McKenna, J., Sanchez-Quinto, F., Bernhardsson, C., Ebeo, C., Reyes, R., Casel, O., Huang, J. Y., Hagada, K. P., Guilay, D., Reyes, J., Allian, F. P., Mori, V., Azarcon, L. S., Manera, A., Terando, C., Jamero, L., Jr, Sireg, G., Manginsay-Tremedal, R., Labos, M. S., Latiph, A., Saway, R.L., Marte, E., Magbanua, P., Morales, A., Java, I., Reveche, R., Barrios, B., Burton, E., Salon, J.C., Kels, M.J.T., Albano, A., Cruz-Angeles, R.B., Molanida, E., Granehäll, L., Vicente, M., Edlund, H., Loo, J.-H., Trejaut, J., Ho, S.Y.W., Reid, L., Lambeck, K., Malmström, H., Schlebusch, C., Endicott, P., Jakobsson, M., in press. Philippine Ayta possess the highest level of Denisovan ancestry in the world. Current Biology. https://doi.org/10.1016/j.cub.2021.07.022.

Lockey, A.L., Alemseged, Z., Hublin, J.J., Skinner, M.M., 2020. Maxillary molar enamel thickness of Plio-Pleistocene hominins. J. Hum. Evol. 142, 102731.

Macchiarelli, R., Bayle, P., Bondioli, L., Mazurier, A., Zanolli, C., 2013. From outer to inner structural morphology in dental anthropology. The integration of the third dimension in the visualization and quantitative analysis of fossil remains. In: Scott, R.G., Irish, J.D. (Eds.), Anthropological Perspectives on Tooth Morphology: Genetics, Evolution, Variation. Cambridge University Press, Cambridge, pp. 250–277.

Martin, L.B., 1985. Significance of enamel thickness in hominoid evolution. Nature 314, 260–263.

Martinez Arbizu, P., 2020. pairwiseAdonis: Pairwise multilevel comparison using Adonis. R package version 0.4. https://github.com/pmartinezarbizu/pairwiseAdonis.

Martín-Francés, L., Martinón-Torres, M., Martínez de Pinillos, M., García-Campos, C., Zanolli, C., Bayle, P., Modesto-Mata, M., Arsuaga, J.L., Bermúdez de Castro, J.M., 2020. Crown tissue proportions and enamel thickness distribution in the Middle Pleistocene hominin molars from Sima de los Huesos (SH) population (Atapuerca, Spain). PLoS One 15, 0233281.

Matsu'ura, S., Kondo, M., Danhara, T., Sakata, S., Iwano, H., Hirata, T., Kurniawan, I., Setiyabudi, E., Takeshita, Y., Hyodo, M., Kitaba, I., Sudo, M., Danhara, Y., Aziz, F., 2020. Age control of the first appearance datum for Javanese *Homo erectus* in the Sangiran area. Science 367, 210–214.

Mijares, A.S.B., 2007. Unearthing Prehistory: The Archaeology of Northeastern Luzon, Philippine Islands. BAR International Series 1613. John and Erica Hedges Ltd., Oxford.

Mijares, A.S.B., Détroit, F., Piper, P., Grün, R., Bellwood, P., Aubert, M., Champion, G., Cuevas, N., De Leon, A., Dizon, E., 2010. New evidence for a 67,000-year-old human presence at Callao Cave, Luzon, Philippines. J. Hum. Evol. 59, 123–132.

Moore, N.C., Skinner, M.M., Hublin, J.J., 2013. Premolar root morphology and metric variation in *Pan troglodytes verus*. Am. J. Phys. Anthropol. 150, 632–646.

Moore, N.C., Hublin, J.J., Skinner, M.M., 2015. Premolar root and canal variation in extant non-human hominoidea. Am. J. Phys. Anthropol. 158, 209–226.

Moore, N.C., Thackeray, J.F., Hublin, J.-J., Skinner, M.M., 2016. Premolar root and canal variation in South African Plio-Pleistocene specimens attributed to *Australopithecus africanus* and *Paranthropus robustus*. J. Hum. Evol. 93, 46–62.

Morwood, M.J., Brown, P., Jatmiko, Sutikna, T., Wahyu Saptomo, E., Westaway, K.E., Awe Due, R., Roberts, R.G., Maeda, T., Wasisto, S., Djubiantono, T., 2005. Further evidence for small-bodied hominins from the Late Pleistocene of Flores, Indonesia. Nature 437, 1012–1017.

Oksanen, J., Blanchet, F.G., Friendly, M., Kindt, R., Legendre, P., McGlinn, D., Minchin, P.R., O'Hara, R.B., Simpson, G.L., Solymos, P., Stevens, M.H.H., Szoecs, E., Wagner, H., 2020. vegan: Community ecology package. R package version 2.5-7. https://CRAN.R-project.org/package=vegan.

Olejniczak, A.J., Smith, T.M., Feeney, R.N.M., Macchiarelli, R., Mazurier, A., Bondioli, L., Rosas, A., Fortea, J., de la Rasilla, M., Garcia-Tabernero, A., Radovčić, J., Skinner, M.M., Toussaint, M., Hublin, J.-J., 2008. Dental tissue proportions and enamel thickness in Neandertal and modern human molars. J. Hum. Evol. 55, 12–23.

Pan, L., Zanolli, C., 2019. Comparative observations on the premolar root and pulp canal configurations of Middle Pleistocene *Homo* in China. Am. J. Phys. Anthropol. 168, 637–646.

Pan, L., Dumoncel, J., Mazurier, A., Zanolli, C., 2019. Structural analysis of premolar roots in Middle Pleistocene hominins from China. J. Hum. Evol. 136, 102669.

Pan, L., Dumoncel, J., Mazurier, A., Zanolli, C., 2020. Hominin diversity in East Asia during the Middle Pleistocene: A premolar endostructural perspective. J. Hum. Evol. 148, 102888.

R Core Team, 2021. R: A language and environment for statistical computing. R Foundation for Statistical Computing, Vienna.

Reich, D., Green, R. E., Kircher, M., Krause, J., Patterson, N., Durand, E. Y., Viola, B., Briggs, A. W., Stenzel, U., Johnson, P. L., Maricic, T., Good, J. M., Marques-Bonet, T., Alkan, C., Fu, Q., Mallick, S., Li, H., Meyer, M., Eichler, E. E., Stoneking, M., Richards, M., Talamo, S., Shunkov, M.V., Derevianko, A.P., Hublin, J.-J., Kelso, J., Slatkin, M., Pääbo, S., 2010. Genetic history of an archaic hominin group from Denisova Cave in Siberia. Nature 468, 1053–1060.

Robles, E., Piper, P., Ochoa, J., Lewis, H., Paz, V., Ronquillo, W., 2015. Late Quaternary sea-level changes and the palaeohistory of Palawan Island, Philippines. J. Island Coast. Archaeol. 10, 76–96.

Sawyer, S., Renaud, G., Viola, B., Hublin, J. J., Gansauge, M. T., Shunkov, M. V., Derevianko, A. P., Prüfer, K., Kelso, J., Pääbo, S., 2015. Nuclear and mitochondrial DNA sequences from two Denisovan individuals. Proc. Natl. Acad. Sci. USA 112, 15696–15700.

Schlager, S., 2020. Morpho: calculations and visualizations related to geometric morphometrics. R package version 2.8. http://cran.r-project.org/web/packages/Morpho/index.html.

Schneider, C.A., Rasband, W.S., Eliceiri, K.W., 2012. NIH Image to ImageJ: 25 years of image analysis. Nat. Methods 9, 671–675.

Scott, G.R., Turner II, C.G., Townsend, G.C., Martinón-Torres, M., 2018. The Anthropology of Modern Human Teeth. Dental Morphology and its Variation in Recent and Fossil *Homo sapiens*, 2nd ed. Cambridge University Press, Cambridge.

Skinner, M.M., Wood, B.A., Boesch, C., Olejniczak, A.J., Rosas, A., Smith, T., Hublin, J.-J., 2008. Dental trait expression at the enamel-dentine junction of lower molars in extant and fossil hominoids. J. Hum. Evol. 54, 173–186.

Skinner, M.M., Gunz, P., Wood, B.A., Boesch, C., Hublin, J.-J., 2009. Discrimination of extant *Pan* species and subspecies using the enamel-dentine junction morphology of lower molars. Am. J. Phys. Anthropol. 140, 234–243.

Skinner, M.M., de Vries, D., Gunz, P., Kupczik, F., Klassen, R.P., Hublin, J.-J., Roksandic, M., 2016. A dental perspective on the taxonomic affinity of the Balanica mandible (BH-1). J. Hum. Evol. 93, 63–81.

Smith, T.M., Olejniczak, A.J., Reh, S., Reid, D.J., Hublin, J.-J., 2008. Brief Communication: Enamel thickness trends in the dental arcade of humans and chimpanzees. Am. J. Phys. Anthropol. 136, 237–241.

Smith, T.M., Houssaye, A., Kullmer, O., Le Cabec, A., Olejniczak, A.J., Schrenk, F., de Vos, J., Tafforeau, P., 2018. Disentangling isolated dental remains of Asian Pleistocene hominins and pongines. PLoS One 13, e0204737.

Sondaar, P.Y., 1991. Island mammals of the past. Sci. Progress 75, 249‑264.

Spoor, C.F., Zonneveld, F.W., Macho, G.A., 1993. Linear measurements of cortical bone and dental enamel by computed tomography: applications and problems. Am. J. Phys. Anthropol. 91, 469–484.

Sutikna, T., Tocheri, M.W., Morwood, M.J.,Wahyu Saptomo, E., Jatmiko, Due Awe, R., Wasisto, S.,Westaway, K.E., Aubert, M., Li, B., Zhao, J.-x, Storey, M., Alloway, B.V., Morley, M.W., Meijer, H.J.M., van den Bergh, G.D., Grün, R., Dosseto, A., Brumm, A., Jungers, W.L., Roberts, R.G., 2016. Revised stratigraphy and chronology for *Homo floresiensis* at Liang Bua in Indonesia. Nature 532, 366–369.

Tocheri, M.W., 2019. Previously unknown human species found in Asia raises questions about early hominin dispersals from Africa. Nature 568, 176–178.

Tocheri, M.W., Orr, C.M., Larson, S.G., Sutikna, T., Jatmiko, Saptomo, E.W., Awe, R.D., Djubiantono, T., Morwood, M.J., Jungers, W.L., 2007. The primitive wrist of *Homo floresiensis* and its implications for hominin evolution. Science 317, 1743–1745.

van den Bergh, G.D., Kaifu, Y., Kurniawan, I., Kono, R.T., Brumm, A., Setiyabudi, E., Aziz, F., Morwood, M.J., 2016. *Homo floresiensis*-like fossils from the early Middle Pleistocene of Flores. Nature 534, 245–248.

van den Hoek Ostende, L.W., 2018. Cladistics and insular evolution, an unfortunate marriage? Another tangle in the *Deinogalerix* analysis of Borrani et al. (2017). Cladistics 34, 708‑713.

van der Geer, A.A.E., 2005. Island ruminants and parallel evolution of functional structures. In: Crégut-Bonnoure, E (Ed.), Les Ongulés Holarctiques du Pliocène et du Pléistocène. Maison de la Géologie, Paris, pp. 231–240.

van der Geer, A.A.E., 2014. Parallel patterns and trends in functional structures in extinct island mammals. Integr. Zool. 9, 167–182.

van der Geer, A.A.E., Lomolino, M.V., Lyras, G.A., 2017. 'Island Life' before man: biogeography of palaeo-insular mammals. J. Biogeogr. 44, 995–1006.

Voris, H.K., 2000. Maps of Pleistocene sea levels in Southeast Asia: shorelines, river systems and time durations. J. Biogeogr. 27, 1153–1167.

Wood, B., Engleman, C., 1988. Analysis of the dental morphology of Plio-Pleistocene hominids. V. Maxillary postcanine tooth morphology. J. Anat. 161, 1–35.

Xing, S., Martinón-Torres, M., Bermúdez de Castro, J.M., Zhang, Y., Fan, X., Zheng, L., Huang, W., Liu, W., 2014. Middle Pleistocene hominin teeth from Longtan Cave, Hexian, China. PLoS One 9, e114265.

Young, C.B., 2020. Static allometry of a small-bodied omnivore: Body size and limb scaling of an island fox and inferences for *Homo floresiensis*. J. Hum. Evol. 149, 102899.

Zanolli, C., 2013. Additional evidence for morpho-dimensional tooth crown variation in a new Indonesian *H. erectus* sample from the Sangiran Dome (Central Java). PLoS One 8, e67233.

Zanolli, C., 2015. Molar crown inner structural organization in Javanese *Homo erectus*. Am. J. Phys. Anthropol. 156, 148–157.

Zanolli, C., Pan, L., Dumoncel, J., Kullmer, O., Kundrát, M., Liu, W., Macchiarelli, R., Mancini, L., Schrenk, F., Tuniz, C., 2018. Inner tooth morphology of *Homo erectus* from Zhoukoudian. New evidence from an old collection housed at Uppsala University, Sweden. J. Hum. Evol. 116, 1–13.

Zanolli, C., Kullmer O., Kelley J., Bacon A.M., Demeter F., Dumoncel J., Fiorenza L., Grine F.E., Hublin J.J., Anh Tuan N., Thi Mai Huong N., Pan L., Schillinger B., Schrenk F., Skinner M.M., Ji X., Macchiarelli R., 2019a. Evidence for increased hominid diversity in the Early-Middle Pleistocene of Indonesia. Nat. Ecol. Evol. 3, 755–764.

Zanolli, C., Biglari, F., Mashkour, M., Abdi, K., Monchot, H., Debue, K., Mazurier, A., Bayle, P., Le Luyer, M., Rougier, H., Trinkaus, E., Macchiarelli, R., 2019. A Neanderthal from the Central Western Zagros, Iran. Structural reassessment of the Wezmeh 1 maxillary premolar. J. Hum. Evol. 135, 102643.

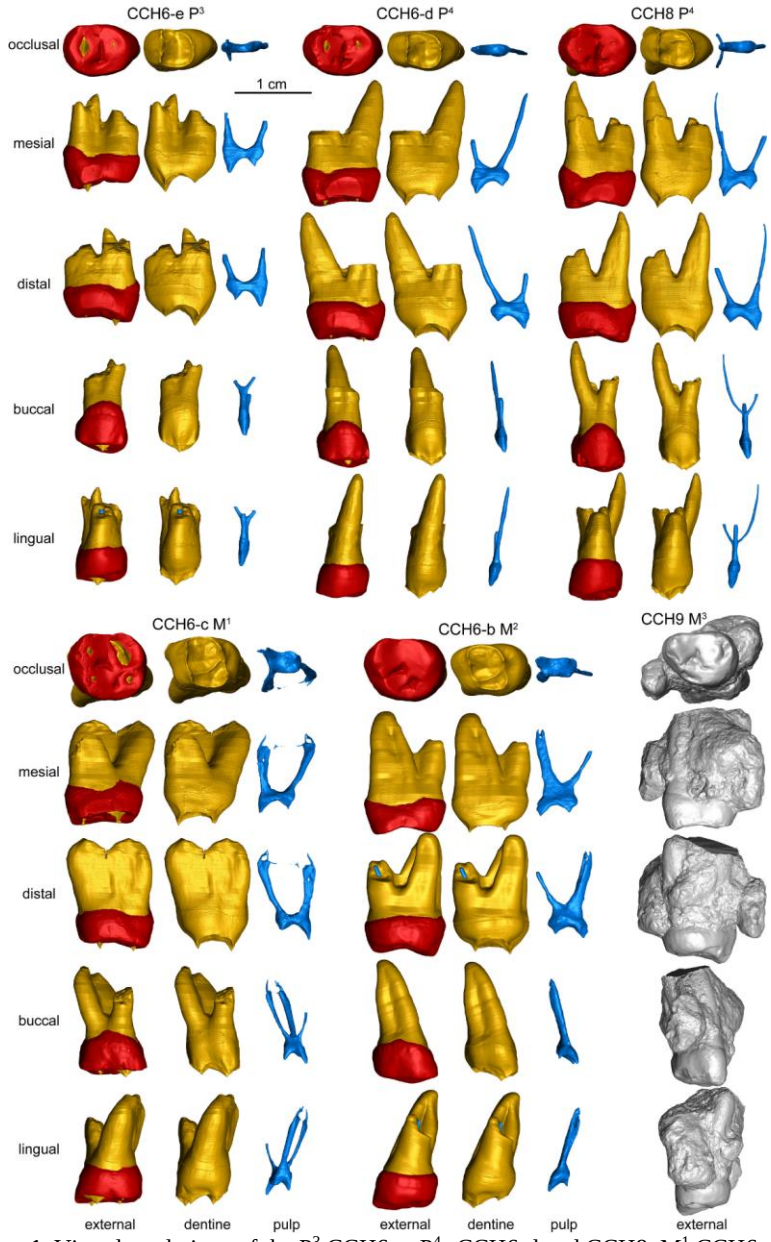

Figure 1. Virtual renderings of the P^3 CCH6-e, P^4s CCH6-d and CCH8, M^1 CCH6-c, M^2

CCH6-b, and M^3 CCH9. Except for the M^3 for which only the external morphology is shown, the external, dentine (with reconstructed dentine horns), and pulp surfaces are illustrated in occlusal, mesial, distal, buccal, and lingual views. To facilitate reading of the figure, all specimens are illustrated as right antimeres.

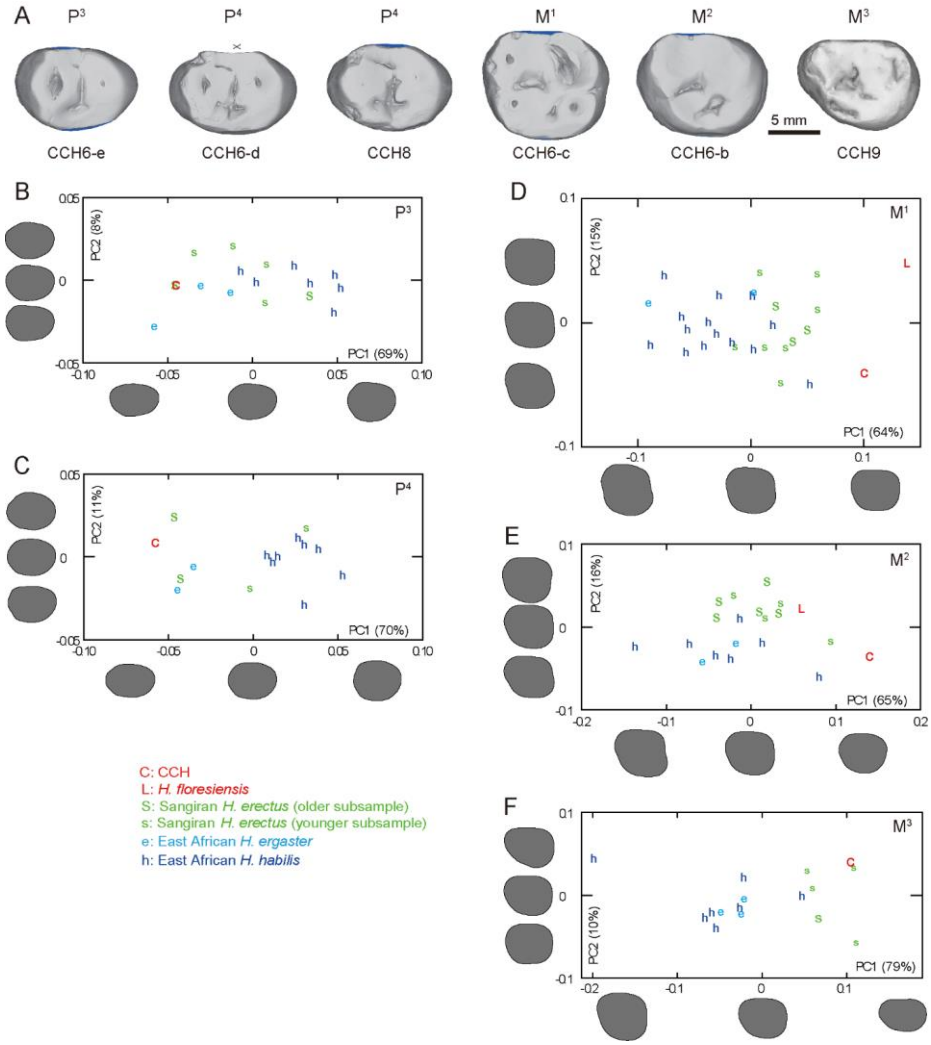

Figure 2. Crown outline analyses. A) Occlusal contours of the maxillary premolars and molars of *Homo luzonensis* from Callao Cave, with the reconstructed areas in blue. Mesial wear on CCH6-d (indicated by an x) is too severe for confident reconstruction and the specimen was not included in the analysis. B–F) Plots of the first and second principal component scores (PC1 and PC2)

derived from the normalized elliptic Fourier analyses for the P^3 (B), P^4 (C), M^1 (D), M^2 (E), and M^3 (F) crown contours of the *Homo luzonensis* teeth compared with Pleistocene *Homo* samples. Considering the significant chronological tooth size reduction trend observed within the Sangiran (Indonesian) *H. erectus* sample (Kaifu et al., 2005b), specimens that are surely or supposedly derived from the Sangiran Formation and the Grenzbank zone (older subsample) are indicated by the uppercase 'S' while those surely or likely deriving from the overlying Bapang Formation (younger subsample) are shown by the lowercase 's'.

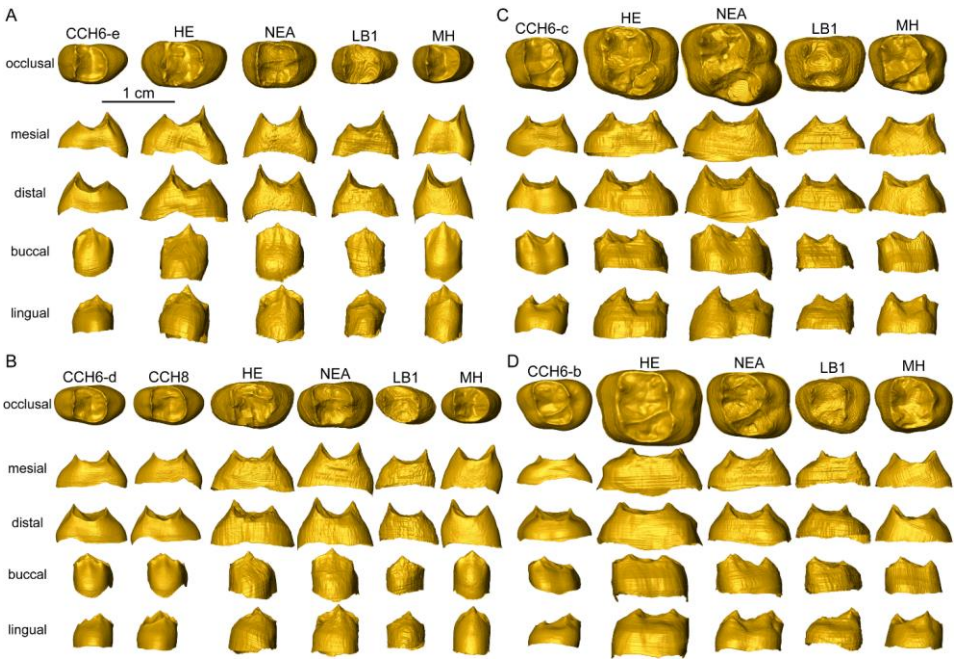

Figure 3. Virtually reconstructed enamel-dentine junction of the *Homo luzonensis* teeth (CCH) compared with those of *Homo erectus* (HE; P^3–M^2 of Sangiran 4), Neanderthals (NEA; P^3 D45, P^4 D39, M^1 D136, M^2 D165), *Homo floresiensis* (LB1) and modern humans (MH) in occlusal, mesial, distal, buccal and lingual views. For comparative purpose, all specimens are illustrated as right antimeres.

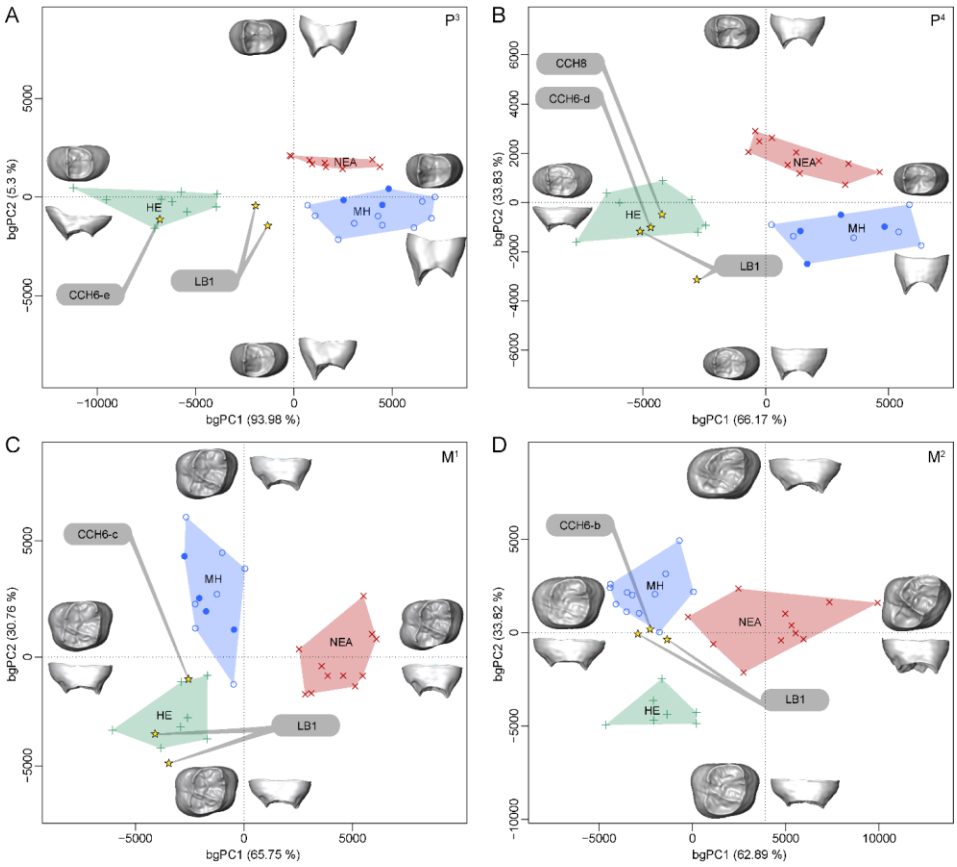

Figure 4. Bivariate plot of the between-group principal component 2 (bgPC2) against the between-group component 1 (bgPC1) based on the diffeomorphic surface matching analyses of the enamel-dentine junction of the *Homo luzonensis* (CCH) and *Homo floresiensis* (LB1) teeth compared with *Homo erectus* (HE), Neanderthals (NEA), and modern humans (MH). The filled circles represent the fossil modern human specimens from Qafzeh. The surfaces at the end of the axes illustrate the extreme shapes along each component.

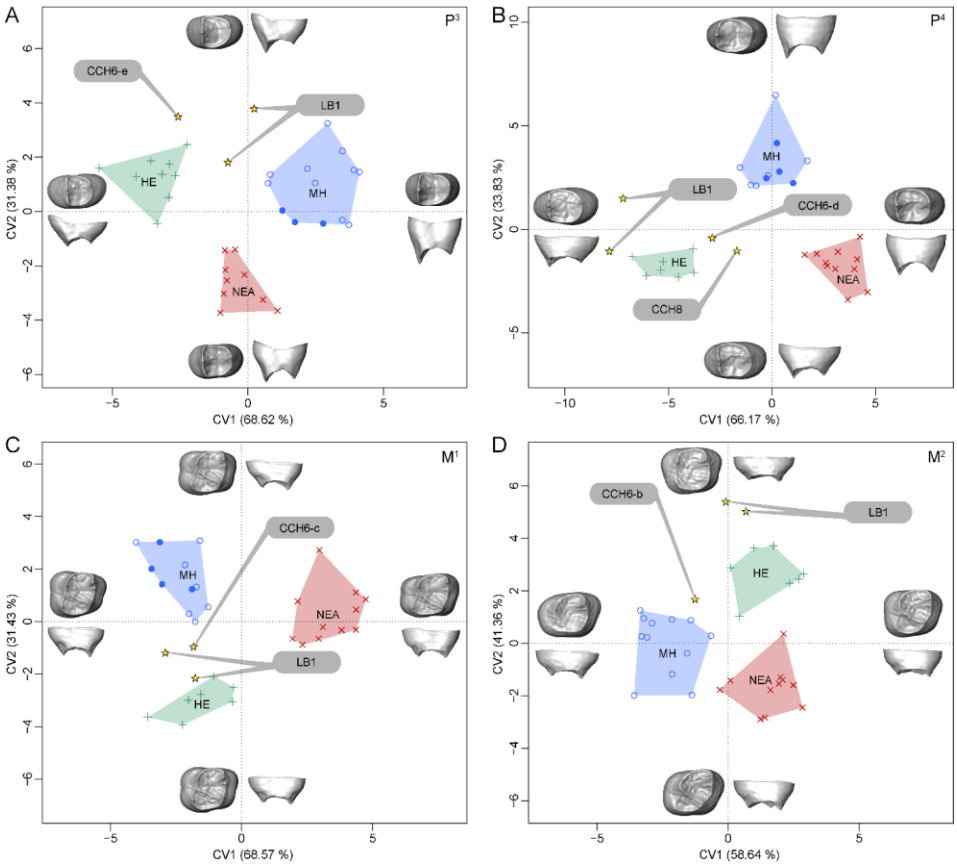

Figure 5. Bivariate plot of the canonical variate 2 (CV2) against the canonical variate 1 (CV1) based on the diffeomorphic surface matching analyses of the enamel-dentine junction of the *Homo luzonensis* (CCH) and *Homo floresiensis* (LB1) teeth compared with *Homo erectus* (HE), Neanderthals (NEA), and modern humans (MH). The filled circles represent the fossil modern human specimens from Qafzeh. The surfaces at the end of the axes illustrate the extreme shapes along each component.

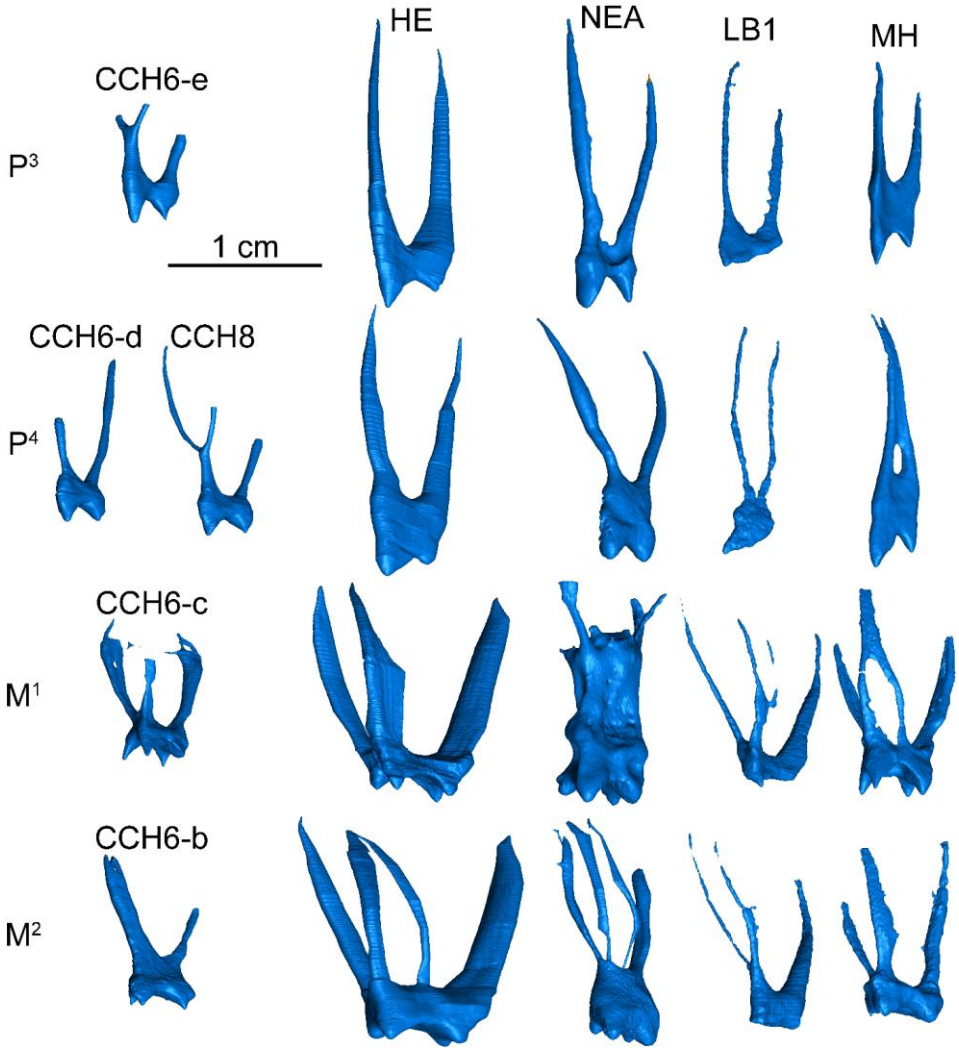

Figure 6. Virtual renderings in mesiobuccal view of the pulp cavity of the *Homo luzonensis* (CCH) teeth compared with those of *Homo erectus* (HE; P^3–M^2 of Sangiran 4), Neanderthals (NEA; P^3 D45, P^4 D39, M^1 D136, M^2 D165), *Homo floresiensis* (LB1), and modern humans (MH).

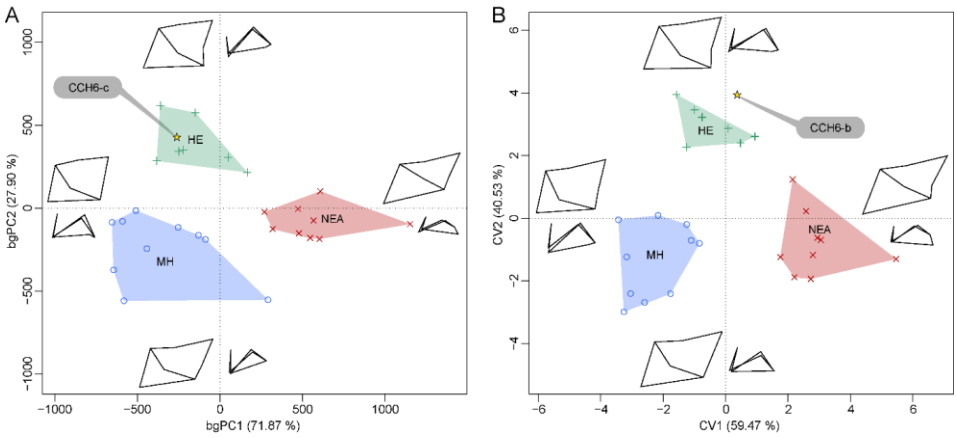

Figure 7. Bivariate plot of the between-group principal component 2 (bgPC2) against the between-group component 1 (bgPC1; A) and of the canonical variate 2 (CV2) against the canonical variate 1 (CV1; B) based on the landmark analysis of the pulp chamber roof of the *Homo luzonensis* M^1 CCH6-c compared with the M^1s of *Homo erectus* (HE), Neanderthals (NEA), and modern humans (MH). The wireframes at the end of the axes illustrate the extreme shapes along each component.

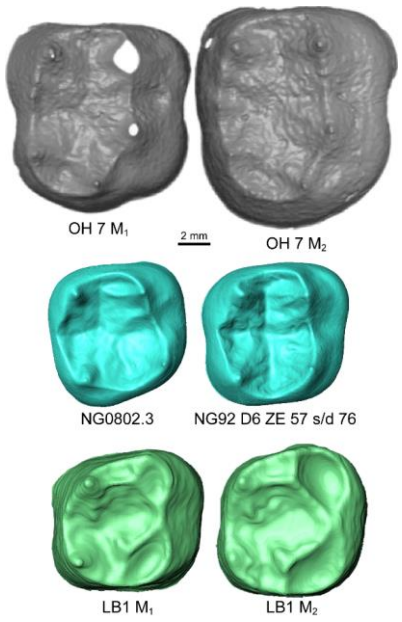

Figure 8. The enamel-dentine junction of the M_1 and M_2 of *Homo habilis* (OH 7; Davies et al., 2021), of late Early to Middle Pleistocene Indonesian *Homo erectus* M_2s (NG0802.3 and NG92 D6 ZE 57s/d 76; Zanolli, 2015), and *Homo floresiensis* M_1 and M_2 (Kaifu et al., 2015b).

Table 1

Bidimensional and three-dimensional average enamel thickness (AET and 3D AET) and relative enamel thickness (RET and 3D RET) indices computed for the *Homo luzonensis* M^2 CCH6-b and compared with Pleistocene and recent *Homo* samples.[a]

		AET (mm)	3D AET (mm)	RET	3D RET
Homo luzonensis	mean	1.11 (1)	1.06 (1)	21.77 (1)	20.57 (1)
African early *Homo*	mean	2.00 (2)		25.42 (2)	
	range	1.72–2.27 (2)		19.30–31.54 (2)	
Homo erectus s.s.	mean	1.47 (2)	1.50 (1)	21.81 (2)	18.70 (1)
	range	1.42–1.51 (2)		20.10–23.52 (2)	
Homo antecessor	mean	1.39 (2)	1.44 (2)	21.74 (2)	21.30 (2)
	range	1.27–1.52 (2)	1.32–1.56 (2)	20.26–23.22 (2)	19.01–23.59 (2)
Middle Pleistocene Neanderthals	mean	1.18 (8)	1.24 (9)	19.62 (8)	20.15 (9)
	SD	0.09 (8)	0.10 (9)	1.69 (8)	1.47 (9)
	range	1.06–1.28 (8)	1.05–1.43 (9)	16.88–22.22 (8)	18.43–23.74 (9)
Late Pleistocene Neanderthals	mean	1.20 (5)	1.05 (5)	18.12 (5)	14.91 (5)
	SD	0.08 (5)	0.08 (5)	1.84 (5)	1.84 (5)
	range	1.13–1.29 (5)	0.96–1.13 (5)	15.65–20.85 (5)	13.24–17.56 (5)
Modern humans	mean	1.4 (25)	1.33 (14)	21.59 (25)	21.93 (14)
	SD	0.17 (25)	0.19 (14)	3.13 (25)	3.94 (14)
	range	1.13–1.76 (25)	0.96–1.78 (14)	16.49–28.03 (25)	15.06–31.63 (14)

[a] The comparative material includes: KNM-ER 1590 and SK 27 for African early *Homo* (Lockey et al., 2020); PA833, Sangiran 4 and Sangiran 7-53 for *H. erectus* s.s. (Xing et al., 2014; Smith et al., 2018; Zanolli et al., 2019a); AT6-12 and AT6-69 for *H. antecessor* (Martín-Francés et al., 2020); AT-12, AT-824, AT-817, AT-15, AT-170, AT-960, AT-822, AT-2175, and AT-6215 for Middle Pleistocene Neanderthals from Sima de los Huesos (Martín-Francés et al., 2020); SR4, SR332, SR531, SR551, and Spy I for Late Pleistocene Neanderthals (Martín-Francés et al., 2020); and modern humans (Martín-Francés et al., 2020).

Table 2

Posterior probabilities based on the between-group principal component analyses (bgPCA) and canonical variate analyses (CVA) of the DSM analyses of the EDJ shape of the *Homo luzonensis* and *Homo floresiensis* specimens.[a]

Tooth	Specimen	MH		NEA		HE	
		bgPCA	CVA	bgPCA	CVA	bgPCA	CVA
P^3	CCH6-e	<0.01	0%	<0.01	0%	**0.35**	**100%**
	LB1 L	0.01	9%	<0.01	0%	**0.08**	**91%**
	LB1 R	**0.01**	**94%**	<0.01	0%	**0.01**	6%
P^4	CCH6-d	<0.01	0%	<0.01	0%	**0.66**	**100%**
	CCH8	<0.01	2%	<0.01	0%	**0.97**	**98%**
	LB1 L	<0.01	0%	<0.01	0%	**0.49**	**100%**
	LB1 R	<0.01	0%	<0.01	0%	**<0.01**	**100%**
M^1	CCH6-c	0.06	20%	<0.01	0%	**0.54**	**80%**
	LB1 L	<0.01	0%	<0.01	0%	**0.45**	**100%**
	LB1 R	<0.01	16%	<0.01	0%	**0.67**	**84%**
M^2	CCH6-b	**0.22**	0%	0.01	1%	<0.01	**99%**
	LB1 L	**0.17**	0%	<0.01	0%	<0.01	**100%**
	LB1 R	**0.06**	0%	0.02	0%	<0.01	**100%**

Abbreviations: DSM = diffeomorphic surface matching; EDJ = enamel-dentine junction; MH = modern humans; NEA = Neanderthals; HE = *Homo erectus* s.l.; L = left; R = right.

[a] Significant values are highlighted in bold. For the bgPCA predictions on the left, the greater the number, the higher the probability and for the CVA predictions on the right, the higher the percentage, the higher the probability.

Commenté [A1]: Add DSM and EDJ to abbreviations

Commenté [A2R1]: Added

Table 3

Maxillary premolar root and canal configuration of *Homo luzonensis* compared with fossil and recent *Homo* samples.[a]

Taxon	Tooth	Specimens	Root-canal formula[b] (frequency)
Homo luzonensis	P^3	CCH6-e	3R: 2_2B+1_1L (1/1)
	P^4	CCH6-d, CCH8	2R: 1_1B+1_1L (1/1); 3R: 2_2B+1_1L (1/1)
Homo erectus	P^3	Sangiran 4, Sangiran 7-35, PA105-4, PA67, PA76, PA524, PA832, Chaoxian, Sh.y.003	$1R_{2(1B+1L)}$ (1/9); 2R: 1_1B+1_1L (6/9); 3R: 2_2B+1_1L (2/9)
	P^4	Sangiran 4, PA68, Chaoxian, Sh.y.007	$1R(Bf)_{1Bf}$ (1/4); $1R_{2(1B+1L)}$ (1/4); 2R: 1_1B+1_1L (2/4)
Neanderthals	P^3	D38, D39, D45, D47, D48, D51, D53, D54, D55	2R: 1_1B+1_1L (9/9)
	P^4	D40, D41, D42, D44, D46, D49, BD 14	$1R_1$ (1/7); 2R: 1_1B+1_1L (6/7)
H. floresiensis	P^3	LB1	$1R_{2(1B+1L)}$ (2/2)
	P^4	LB1	$1R_{2(1B+1L)}$ (2/2)
Modern humans	P^3	*n* = 430	$1R_1$ (108/430); $1R_{2(1B+1L)}$ (90/430); 2R: 1_1B+1_1L (221/430); 3R: 2_2B+1_1L (11/430)
	P^4	*n* = 363	$1R_1$ (147/363); $1R_{2(1B+1L)}$ (163/363); 2R: 1_1B+1_1L (58/363); 3R: 2_2B+1_1L (6/363)

Abbreviations: R = root branch; B = buccal; L = lingual.

[a] Data for fossil specimens were extracted from Pan and Zanolli (2019) except Sangiran 7-35 (original data), while those for modern humans are from Abella et al. (2015).

[b] Column standard numbers denote root number and subscript numbers denote canal number.

Table 4

Posterior probabilities based on the between-group principal component analyses (bgPCA) and canonical variate analyses (CVA) of the landmark-based analyses of pulp shape of CCH6-c.[a]

Tooth	Specimen	MH		NEA		HE	
		bgPCA	CVA	bgPCA	CVA	bgPCA	CVA
M^1	CCH6-c	<0.01	0%	<0.01	0%	**0.92**	**100%**

Abbreviations: MH = modern humans; NEA = Neanderthals; HE = *Homo erectus* s.l.

[a] Significant values are highlighted in bold (for the bgPCA predictions on the left, the greater the number, the higher the probability and for the CVA predictions on the right, the higher the percentage, the higher the probability).